Cdon deficiency causes cardiac remodeling through hyperactivation of WNT/β-catenin signaling

Myong-Ho Jeong[a,b,1], Hyun-Ji Kim[b,c,1], Jung-Hoon Pyun[a,b], Kyu-Sil Choi[b], Dong I. Lee[d], Soroosh Solhjoo[d], Brian O'Rourke[d], Gordon F. Tomaselli[d], Dong Seop Jeong[e], Hana Cho[b,c,2], and Jong-Sun Kang[a,b,2]

[a]Department of Molecular Cell Biology, Sungkyunkwan University School of Medicine, Suwon, Korea 16419; [b]Samsung Biomedical Research Institute, Samsung Medical Center, Sungkyunkwan University School of Medicine, Seoul, Korea 06351; [c]Department of Physiology, Sungkyunkwan University School of Medicine, Suwon, Korea 16419; [d]Division of Cardiology, Department of Medicine, Johns Hopkins University School of Medicine, Baltimore, MD 21205; and [e]Department of Thoracic and Cardiovascular Surgery, Samsung Medical Center, Sungkyunkwan University School of Medicine, Seoul, Korea 06351

Edited by Eric N. Olson, University of Texas Southwestern Medical Center, Dallas, TX, and approved January 4, 2017 (received for review September 9, 2016)

On pathological stress, Wnt signaling is reactivated and induces genes associated with cardiac remodeling and fibrosis. We have previously shown that a cell surface receptor Cdon (cell-adhesion associated, oncogene regulated) suppresses Wnt signaling to promote neuronal differentiation however its role in heart is unknown. Here, we demonstrate a critical role of Cdon in cardiac function and remodeling. Cdon is expressed and predominantly localized at intercalated disk in both mouse and human hearts. Cdon-deficient mice develop cardiac dysfunction including reduced ejection fraction and ECG abnormalities. *Cdon*$^{-/-}$ hearts exhibit increased fibrosis and up-regulation of genes associated with cardiac remodeling and fibrosis. Electrical remodeling was demonstrated by up-regulation and mislocalization of the gap junction protein, Connexin 43 (Cx43) in *Cdon*$^{-/-}$ hearts. In agreement with altered Cx43 expression, functional analysis both using *Cdon*$^{-/-}$ cardiomyocytes and shRNA-mediated knockdown in rat cardiomyocytes shows aberrant gap junction activities. Analysis of the underlying mechanism reveals that *Cdon*$^{-/-}$ hearts exhibit hyperactive Wnt signaling as evident by β-catenin accumulation and Axin2 up-regulation. On the other hand, the treatment of rat cardiomyocytes with a Wnt activator TWS119 reduces Cdon levels and aberrant Cx43 activities, similarly to Cdon-deficient cardiomyocytes, suggesting a negative feedback between Cdon and Wnt signaling. Finally, inhibition of Wnt/β-catenin signaling by XAV939, IWP2 or dickkopf (DKK)1 prevented Cdon depletion-induced up-regulation of collagen 1a and Cx43. Taken together, these results demonstrate that Cdon deficiency causes hyperactive Wnt signaling leading to aberrant intercellular coupling and cardiac fibrosis. Cdon exhibits great potential as a target for the treatment of cardiac fibrosis and cardiomyopathy.

Cdon | gap junction | connexin 43 | cardiac fibrosis | Wnt

Various forms of cardiac injury signals cause a process called cardiac remodeling, associated with hypertrophy and fibrosis, which is the major independent risk factor for heart failure (1–3). After cardiac injury, distinct fetal signaling pathways such as Wnt signaling are reactivated, which contribute to the development of cardiac remodeling, hypertrophy, and fibrosis (4–8). Wnt signaling can be characterized by canonical (β-catenin dependent) and noncanonical (β-catenin independent) pathways (8). In the canonical Wnt signaling (referred to as "Wnt signaling" hereafter), the binding of Wnt ligand to frizzled receptor and coreceptor lipoprotein receptor-related protein (LRP)5/6 initiates a signaling cascade, resulting in inhibition of glycogen synthase kinase 3β (GSK3β) and nuclear β-catenin accumulation, where it activates target gene expression together with the transcription factor 4 (TCF)/lymphoid enhancer binding factor (LEF) group of transcription factors (9). Wnt signaling plays diverse roles in the control of proliferation and differentiation of cardiac progenitors during heart development (10) and in cardiac remodeling (11). Consistently, inhibition of Wnt signaling significantly reduces cardiac remodeling, postinfarct mortality, and cardiac function decline (12), whereas its activation causes a progressive dilated cardiomyopathy (13, 14). Thus, modulation of Wnt signaling activity might be critical for prevention of maladaptive cardiac remodeling.

The disorganization of the cardiac intercalated disc (ID) has been considered as a "hallmark" of cardiac disease (15–19), whereas the proper organization of junctions at the ID is critical for synchronous contractile function of cardiomyocytes. A "hybrid adhering junction" or "area composita" is a mixing of adherens junctional and desmosomal components, supporting the mechanical load on the mammalian heart by anchoring both actin and intermediate filaments over an extended junctional area at the ID (20, 21). On the other hand, gap junctions provide electrical coupling by a channel composed of connexin 43 (Cx43) that conduct ions and small molecules between adjacent cardiomyocytes (22). Perturbation of gap junction localization and/or activities has been observed in various forms of cardiac diseases (23) and Wnt signaling may be involved in this process through regulation of Cx43 expression and function (24). However, to date, the regulatory mechanisms of the ID's structural remodeling are incompletely understood.

Cdon belongs to the Ig/fibronectin type III subfamily of cell adhesion molecule. Previous studies with Cdon-deficient mice demonstrated critical functions of Cdon in the development of the central nervous system and skeletal muscle via regulation of sonic hedgehog (Shh) and N-cadherin/cell adhesion signaling

Significance

Upon injury, reactivated Wnt/β-catenin signaling is implicated in cardiac remodeling and cardiomyopathy, thus it is an attractive target for intervention of cardiac diseases. Here, we demonstrate a role of a cell surface receptor Cdon in preventing cardiac remodeling through suppression of Wnt signaling. *Cdon*$^{-/-}$ mice develop cardiac dysfunction and fibrosis with altered expression of remodeling genes. Cdon deficiency causes aberrant localization and function of gap junction protein connexin 43, correlating with hyperactivated Wnt signaling. Blocking of Wnt signaling in Cdon-depleted cardiomyocytes attenuates aberrant intercellular coupling. Conversely, Wnt activator causes aberrant activation of gap junction with decreased Cdon levels, suggestive of a feedback mechanism. These data suggest that Cdon is required for the control of Wnt signaling to prevent cardiac remodeling.

Author contributions: M.-H.J., H.-J.K., J.-H.P., K.-S.C., D.I.L., S.S., B.O., G.F.T., D.S.J., H.C., and J.-S.K. designed research; M.-H.J., H.-J.K., J.-H.P., K.-S.C., D.I.L., S.S., and D.S.J. performed research; M.-H.J., H.-J.K., J.-H.P., K.-S.C., D.I.L., S.S., B.O., G.F.T., D.S.J., H.C., and J.-S.K. analyzed data; and M.-H.J., H.-J.K., H.C., and J.-S.K. wrote the paper.

The authors declare no conflict of interest.

This article is a PNAS Direct Submission.

[1]M.-H.J. and H.-J.K. contributed equally to this work.

[2]To whom correspondence may be addressed. Email: kangj01@skku.edu or hanacho@skku.edu.

This article contains supporting information online at www.pnas.org/lookup/suppl/doi:10.1073/pnas.1615105114/-/DCSupplemental.

(25–29). Recently, we have shown that Cdon negatively regulates Wnt signaling to promote neuronal differentiation and ventral cell fate determination in forebrain development (28). The mechanistic study has revealed that Cdon suppresses Wnt signaling through interaction with the LRP6 coreceptor. Even though these signaling pathways play essential roles in cardiac development and function, Cdon's function in heart muscle is still uncharacterized. These facts led us to examine the role of Cdon in cardiac function by using cultured primary cardiomyocytes and Cdon-deficient mice.

Here we demonstrate that Cdon deficiency causes defects in cardiac function and fibrosis. Cdon-deficient hearts exhibit alterations in global gene expression profile and genes involved in cardiac remodeling and stress signals are greatly altered. Specifically, Cx43 proteins are found to be pathologically mislocalized to the lateral sides of *Cdon*$^{-/-}$ cardiomyocytes. In addition, overall Cx43 protein levels are markedly increased in *Cdon*$^{-/-}$ hearts, which likely is associated with hyperactive Wnt signaling. In neonatal rat cardiomyocytes, the treatment of Wnt signaling inhibitors prevents the Cdon-knockdown–induced dysregulation of intercellular coupling and up-regulation of Axin2, collagen1, and Cx43 expression. These data suggest that Cdon is required for maintenance of intercellular coupling and prevention of cardiac fibrosis via suppressing Wnt signaling.

Results

Cdon Is Expressed in Hearts and Predominantly Localized at Intercalate Discs. To examine the role of Cdon in cardiac function, the expression of Cdon was analyzed. Cdon protein was constantly expressed in heart extracts from postnatal day 1 (P1), P7 and P14 mice, along with cardiac junctional proteins, N-cadherin, Cx43, Zonula Occuldens-1 (ZO-1), and α-Catenin (Fig. 1*A*). Immunostaining analysis with Cdon and α-Actinin antibodies on using mouse and human heart sections revealed that Cdon proteins were specifically accumulated at the ID in α-Actinin-positive cardiomyocytes of mouse (5 mo) and normal human hearts (Fig. 1*B*). Additional immunostaining analysis revealed the enrichment of Cdon at the ID together with other junctional proteins, N-cadherin, Cx43, and ZO-1 in mouse and human hearts (Fig. 1 *C* and *D*). The immunofluorescence intensity was quantified in the range of 13-μm vectors bisecting the ID area and the immunofluorescence signals for N-cadherin, Cx43, or ZO-1 overlapped with Cdon virtually in the ID area (Fig. 1 *C* and *D*, *Inset*). In addition, the colocalization probability of Cdon with N-cadherin, Cx43, or ZO-1 was quantified with Pearson's coefficient using ZEN software. In light of the fact that the values above 0.5 are considered to be significant (30), the coefficients ranging from 0.66 to 0.92 support a significant colocalization of these proteins (Fig. 1 *C* and *D*). In contrast, little or no Cdon signals were detected in cardiac fibroblasts positive for discoidin domain receptor 2 (DDR2) (*SI Appendix*, Fig. 1*A*). Consistently, Cdon expression was predominant in neonatal rat ventricular myocytes (NRVMs), compared with neonatal rat cardiac fibroblasts (NRCFs) (*SI Appendix*, Fig. 1*B*). These data suggest that Cdon proteins are enriched at IDs of cardiac myocytes and colocalized with ID proteins, including Cx43.

Cdon Deficiency Causes Impaired Cardiac Function. The histological analysis of hearts from neonatal control *Cdon*$^{+/-}$ and *Cdon*$^{-/-}$ littermates indicated no signs of gross malformation of heart (*SI Appendix*, Fig. 2) and the relative heart weight to body weight was slightly but not significantly increased in neonatal *Cdon*$^{-/-}$ mice (*SI Appendix*, Fig. 2 *A–C*). Consistently, TUNEL assay revealed no alteration in cell survival in neonatal *Cdon*$^{-/-}$ hearts (*SI Appendix*, Fig. 2*D*). The majority of Cdon-deficient mice died around 3 wk of age (26) (Fig. 2*A*).

Electrocardiograms (ECGs) recorded with the animals sedated reveal no significant change in heart rate (HR) and QRS duration but a significantly shorter corrected QT (QTc) interval in the *Cdon*$^{-/-}$ mice (Fig. 2 *B* and *C*). Representative ECGs from WT and *Cdon*$^{-/-}$ mice at 2 wk of age are shown in Fig. 2*B*. QT interval was 38.6 ± 2.1 ms (100.8 ± 9.8 ms corrected for heart rate, $n = 9$) in WT mice and decreased to 29 ± 2.1 ms (79.7 ± 7.1 ms corrected for heart rate, $n = 12$, $P < 0.05$) in *Cdon*$^{-/-}$ mice (Fig. 2 *B* and *C* and *SI Appendix*, Table 1). In addition, ECGs of 11 of 12 *Cdon*$^{-/-}$ mice, tested at random, revealed significant rhythm disturbances (Fig. 2 *D–F*). Junctional tachycardia was the most common arrhythmia, observed in 6 of 12 *Cdon*$^{-/-}$ mice. In addition, three *Cdon*$^{-/-}$ mice displayed 3° atrioventricular (AV)

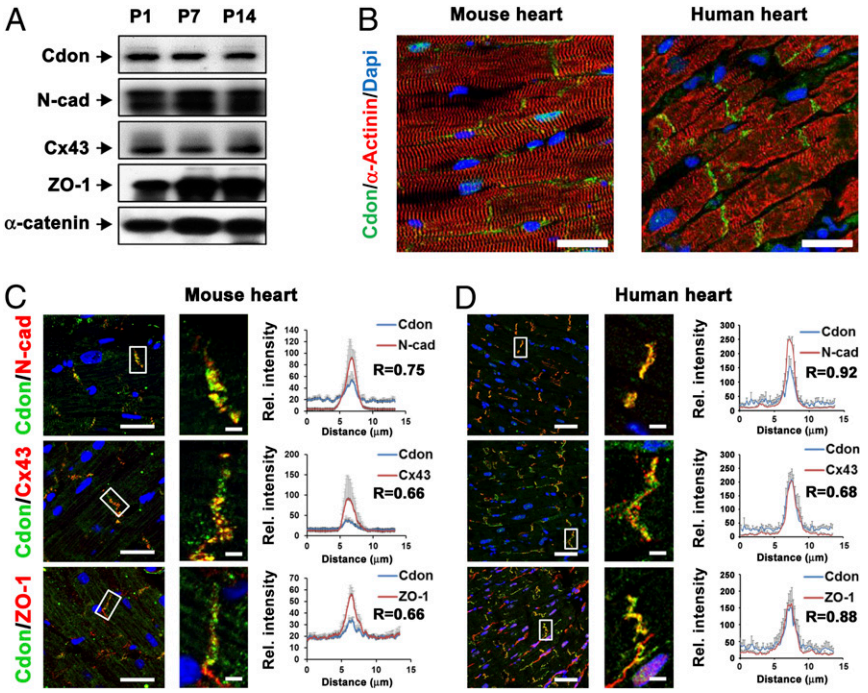

Fig. 1. Cdon is an ID protein and forms complex with N-cadherin. (*A*) Immunoblot analysis for Cdon, N-cadherin (N-cad), Connexin 43, (Cx43), Zonula occludens-1 (ZO-1) and α-catenin in 5-mo-old mouse hearts. (*B*) Representative confocal microscopic images of Cdon and α-actinin staining in mouse (5 mo) and human heart section. (Scale bar, 50 μm.) (*C* and *D*) Immunostaining of Cdon with junctional proteins, N-cad, Cx43, and ZO-1 in mouse and human heart section. (Scale bar, 50 μm.) Magnified images indicating colocalization of Cdon and junctional proteins are shown in the white boxes. (Scale bar, 2.5 μm.) Quantificational analysis for colocalization of Cdon and gap junction proteins and Pearson's correlation coefficients (R) are shown in *C* and *D*, *Right*. Significances of colocalization coefficients were considered as >0.5. ($n = 10$, 10 and 7 for N-cad, Cx43, and ZO-1, respectively, in mouse or $n = 42$, 33, and 40 for N-cad, Cx43, and ZO-1, respectively, in human).

block, and premature ventricular contraction (PVC) was observed in two $Cdon^{-/-}$ mice. In contrast, the total of 15 WT mice tested showed no abnormalities in ECGs. $Cdon^{+/-}$ mice exhibited no difference in HR, QRS duration, and QT interval, compared with WT (*SI Appendix*, Fig. 3 and Table 1), consistent with no visible structural abnormality and survival results.

When the effect of Cdon deficiency on cardiac function was assessed by echocardiograms, 2-wk-old $Cdon^{-/-}$ mice displayed alterations in cardiac function compared with control $Cdon^{+/+}$ littermates (Fig. 2 *G* and *H*). The ejection fraction and the fractional shortening were decreased significantly in $Cdon^{-/-}$ hearts compared with those of $Cdon^{+/+}$ hearts. $Cdon^{-/-}$ mice showed a reduction in the interventricular septum diastole (IVS;d) dimension and posterior wall left ventricular wall thickness in both systole and diastole (LVPW;d or LVPW;s), relative to $Cdon^{+/+}$ mice. Left ventricular dimensions were not different between these mice. These data suggest that Cdon-deficient mice exhibit impaired cardiac function and electrophysiological remodeling.

Cdon-Deficient Hearts Exhibit Alterations in Gene Expression Profiles Associated with Cardiac Remodeling and Fibrosis. To examine the molecular alterations caused by Cdon deficiency, global gene expression profile was assessed by RNA sequencing with hearts from neonatal $Cdon^{+/+}$ and $Cdon^{-/-}$ littermates. From 24,421 initial probes, we identified 239 significantly increased and 207 significantly deceased genes in $Cdon^{-/-}$ neonatal heart compared with $Cdon^{+/+}$ heart sample (>1.3-fold, average of normalized RC log2 >2, *P* value <0.05 with biological repeat, Fig. 3*A*). Next, we performed the gene-annotation enrichment analysis to find functional annotation clustering with the DAVID informatics tool (DAVID Bioinformatics Resources 6.8, National Institute of Allergy and Infectious Diseases/NIH) based on Gene Ontology (GO). Using the 446 differentially regulated genes, we identified nine biological GO terms such as "cell adhesion," "regulation of transferase activity," and "regulation of cell motion," consistent with the proposed role of Cdon (31–33) (Fig. 3 *B* and *C* and *SI Appendix*, Table 2).

To analyze additional signaling pathways altered in Cdon-deficient hearts, we performed the Kyoto Encyclopedia of Genes and Genomes (KEGG) pathway analysis with RNA sequencing data (>1.3-fold, average of normalized RC log2 >2, *P* value <0.05). Genes involved in the metabolic pathway, the PI3K-Akt, regulation of actin cytoskeleton, MAPK, RAP1, and RAS signaling pathways were altered in $Cdon^{-/-}$ hearts (*SI Appendix*, Table 3). Among altered genes, genes implicated in apoptosis, cell cycle, sarcomere, signal transduction (*SI Appendix*, Fig. 4), as well as genes involved in cardiac remodeling and injury (Fig. 3*D*), are shown as heat maps. More specifically, this heat map revealed that Cdon-deficient hearts exhibited elevated expression of genes associated with cardiac remodeling involved in heart injury and myocardial fibrosis, such as connective tissue growth factor (Ctgf), natriuretic peptide B (Nppb), collagen type IV alpha 3 chain (Col4a3), Angiotensin converting enzyme (Ace), and TIMP metallopeptidase inhibitor 3 (Timp3), relative to wild-type hearts (Fig. 3*D*), which are further confirmed by quantitative RT-PCR (qRT-PCR) analysis (Fig. 3*E*). To assess signs of cardiomyopathy, $Cdon^{+/+}$ and $Cdon^{-/-}$ P1 hearts were stained for Masson's trichrome, which revealed that Cdon deficiency causes fibrosis (Fig. 3*F*) with a sevenfold increase,

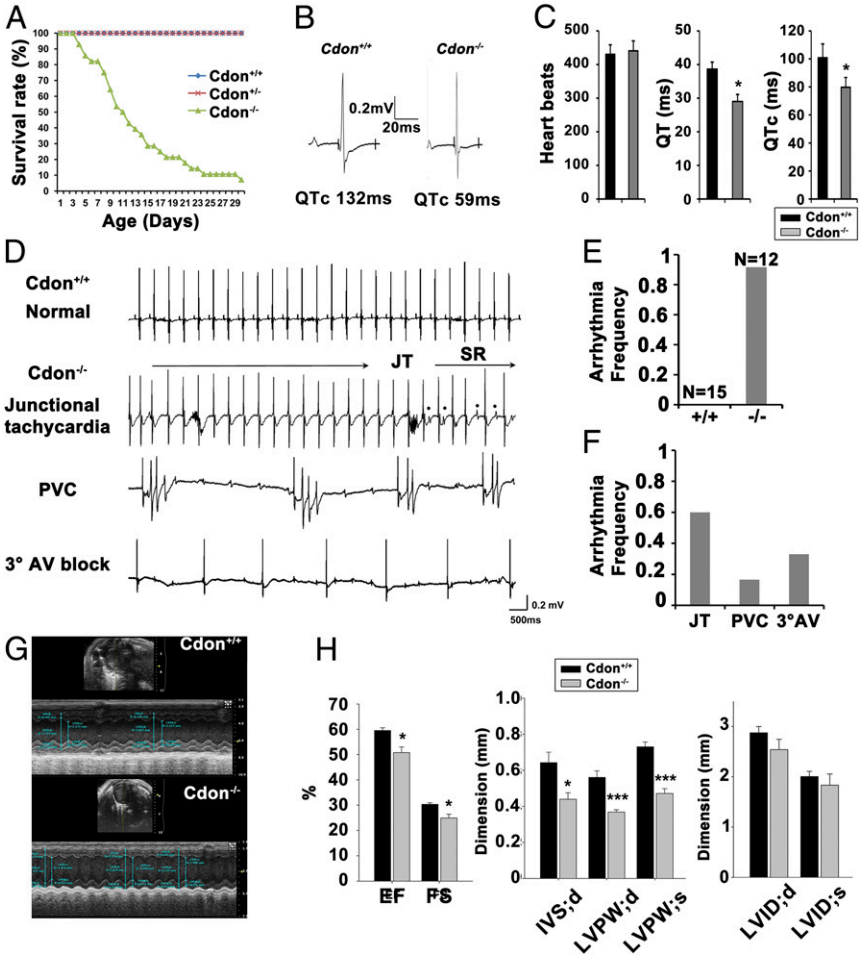

Fig. 2. Cdon deficiency causes impaired cardiac function. (*A*) Survival rate of $Cdon^{+/+}$, $Cdon^{+/-}$, and $Cdon^{-/-}$ mouse during postnatal days 1–30. (*B* and *C*) Electrocardiogram of 2-wk-old $Cdon^{+/+}$ and $Cdon^{-/-}$ mice. Note that QT (QTc) was decreased from 38.6 ± 2.1 ms (QTc: 100.8 ± 9.8 ms, $n = 8$) to 29 ± 2.1 ms (QTc: 79.7 ± 7.1 ms, $n = 7$, $P < 0.05$) in $Cdon^{-/-}$ mice, relative to WT. (*D*) $Cdon^{-/-}$ mice exhibit a wide range of arrhythmias, compared with WT (*Top*). Shown are records of junctional tachycardia (JT), premature ventricular contraction (PVC), and sustained 3° atrioventricular (AV) block. (*E* and *F*) The quantificational analysis for arrhythmia frequency of $Cdon^{+/+}$ and $Cdon^{-/-}$. *, P wave. (*G* and *H*) Representative examples of the short axis transthoracic M mode echocardiographic tracings in $Cdon^{+/+}$ and $Cdon^{-/-}$ mice at postnatal day 14. IVS;d: the interventricular septum; diastolic, LVID;d or LVID;s: the internal dimension of left ventricle (LV); diastolic or systolic, LVPW;d or LVPW;s: the postwall thickness of LV; diastolic or systolic. EF, the ejection fraction; FS, the fraction shortening, Significant *P* values are shown. $n = 5$. *$P < 0.05$, *** $P < 0.005$.

compared with control heart assessed by ImageJ (Fig. 3*G*). Additional Sirius Red staining and Masson's trichrome staining reveal global collagen disposition in LV, IVS, and the apex area in *Cdon*$^{-/-}$ hearts (*SI Appendix*, Fig. 5). These data suggest that Cdon deficiency causes cardiac fibrosis with altered gene expression profiles associated with cardiac remodeling and fibrosis.

Cdon Deficiency Causes Mislocalization of Cx43 Proteins Correlating with Aberrant Gap Junction Activity. The aberrant localization and protein expression of Cx43 have been frequently associated with cardiac remodeling and fibrosis (34, 35). Whereas the presence of Cx43 at the ID is required for proper cardiac conduction, the lateralization and altered levels of this protein have been linked to cardiac pathology (36). To assess potential changes in the expression and localization of Cx43 proteins in the hearts of *Cdon*$^{-/-}$ mice, hearts from 2-wk-old control and *Cdon*$^{-/-}$ mice were subjected to immunostaining for Cx43 (green) and N-cadherin (red) as a marker of the ID. Compared with control heart sections, *Cdon*$^{-/-}$ cardiomyocytes exhibited mislocalization of Cx43 at the lateral borders (Fig. 4*A*). Altered Cx43 localization was observed throughout *Cdon*$^{-/-}$ hearts, such as LV, IVS, and apex regions (*SI Appendix*, Fig. 6). The overlay image of Cx43

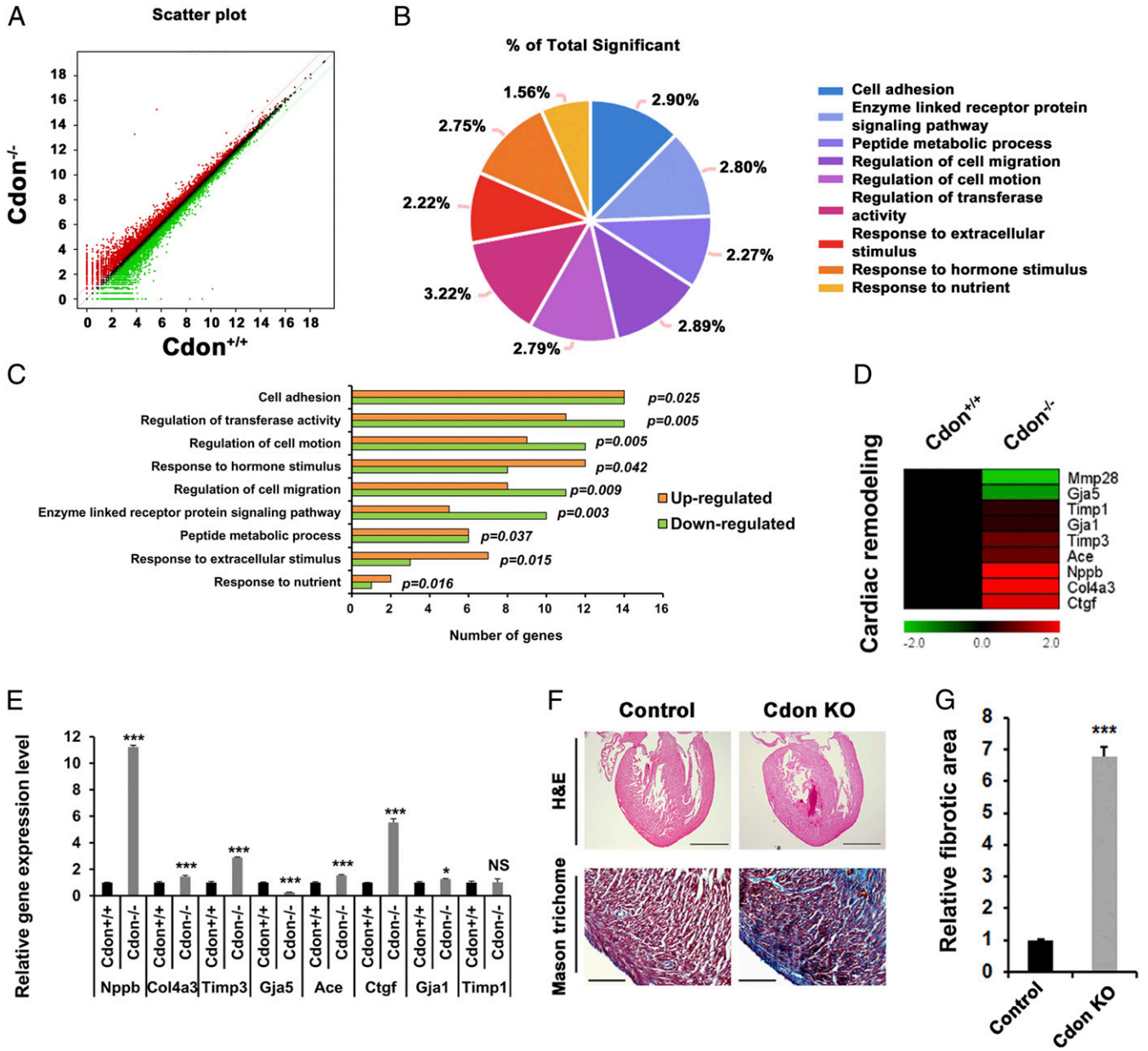

Fig. 3. Increased expression of cardiomyofibrosis and cardiac remodeling genes in neonatal mice lacking Cdon. RNA sequencing analysis with RNAs isolated from *Cdon*$^{+/+}$ and *Cdon*$^{-/-}$ neonatal hearts with biological repeat are shown in *A*–*D*. (*A*) Scatterplot images of RNA sequencing. Red and green color indicate up- and down-regulated genes in *Cdon*$^{-/-}$ hearts, respectively (log twofold change). Black dots indicate genes with no significant change of RNA expression level (less than log twofold change). (*B* and *C*) Venn diagram analysis for altered gene expression of *Cdon*$^{-/-}$ hearts, compared with *Cdon*$^{+/+}$ hearts. The percentage of total significance is presented in *B*, and the graphical analyses of the number of up- and down-regulated genes in Gene Ontology are shown in *C*. (*D*) Heat map for RNA expression level of cardiac remodeling genes. (*E*) Confirmation qPCR analysis for cardiac remodeling genes in *D*. $n = 3$. $^{*}P < 0.05$ and $^{***}P < 0.005$. NS, no significance. (*F*) Histological analysis of the *Cdon*$^{+/-}$ and the *Cdon*$^{-/-}$ mouse hearts at P1. Representative images of H&E and Masson's trichrome staining. [Scale bar, 500 μm (*Upper*), 100 μm (*Lower*).] (*G*) Quantification of fibrotic area in *F*. $n = 3$. $^{***}P < 0.005$.

and N-cadherin of $Cdon^{-/-}$ cardiomyocytes reveals that many of Cx43 proteins are no longer localized at the ID. The mean number of Cx43-immunoreactive puncta was significantly higher in $Cdon^{-/-}$ hearts compared with controls (Fig. 4*B*). This finding was further confirmed with isolated ventricular cardiomyocytes. $Cdon^{-/-}$ cardiomyocytes clearly showed Cx43 staining at the lateral side, whereas Cx43 proteins are largely colocalized with N-cadherin at the cell pole of $Cdon^{+/+}$ myocytes (Fig. 4*C*). The quantification of Cx43 signals showed about twofold increase of Cx43 lateralization in $Cdon^{-/-}$ myocytes (Fig. 4*D*). Western blot analysis confirmed up-regulation of Cx43 and other proteins responsible for cell–cell junctions, including N-cadherin and ZO-1 in $Cdon^{-/-}$ cardiomyocytes, compared with the control (Fig. 4 *E* and *F*). Consistent with the general enhancement of Cx43 levels, both the fast (hypophosphorylated) and slow (hyperphosphorylated) migrating forms of Cx43 proteins are increased. Again, the level of Cx43 recognized by a phosphorylation-specific antibody against serine 368 residue increased (*SI Appendix*, Fig. 7) and this increase is likely due to the general increase of total Cx43.

We next examined whether the up-regulation and lateralization of Cx43 by Cdon deficiency has a functional consequence on intercellular coupling. Because gap junction channels composed of Cx43 are highly permeable to the fluorescent dye Lucifer Yellow (LY), we tested the extent of intercellular LY dye transfer to assess gap junction activity (37). The LY transfer from a single injected cell (marked with yellow line) to an adjacent recipient (marked with red line) in the end-to-end or side-to-side fashion was measured and LY microinjection images of WT and $Cdon^{-/-}$ myocytes at 1, 78, and 126 s are shown (Fig. 4 *G*–*J*). Under normal conditions, the transverse (side to side) electrical coupling is much slower, due to sparse gap junctions at lateral cell borders compared with longitudinal (end to end) coupling (38). Thus, LY dye transfer was much faster in end-to-end cell pairs (Fig. 4*G*, *Upper*) than that in side-to-side cell pairs of WT myocytes (Fig. 4*I*, *Upper*). To analyze the dye transfer, the time course data of the fluorescence intensity in the recipient cell was normalized to the plateau signal intensity and fitted with a single exponential curve (Fig. 4 *H* and *J*). In $Cdon^{-/-}$ myocytes, the side-to-side coupling was strongly increased (Fig. 4 *I*, *Lower* and *J*), whereas the end-to-end coupling was unchanged, relative to the WT myocytes (Fig. 4 *G*, *Lower* and *H*). It is of note that the mean time constant for side-to-side dye transfer in $Cdon^{-/-}$ myocytes is much smaller than that in WT myocytes (Fig. 4*J*, *Right*). Taken together, these data imply that Cdon deficiency causes mislocalization of Cx43 at lateral borders of cardiomyocytes, leading to increased side-to-side coupling between cardiac myocytes.

Ion channel remodeling is often observed in cardiomyopathy and thought to be related to increased arrhythmogenecity (39). We found that both atrial and ventricular myocytes from $Cdon^{-/-}$ mice exhibited action potential duration (APD) shortening (*SI Appendix*, Fig. 8 *A* and *B*). APs were elicited in the whole-cell configuration of the patch clamp by applying depolarizing current pulses over a range of stimulation frequencies. Resting membrane potentials and AP amplitudes were not different between WT and $Cdon^{-/-}$ myocytes. Thus, we hypothesized that shorter APDs in $Cdon^{-/-}$ myocytes were due to remodeling of certain repolarizing currents.

Previous studies have shown that transient outward K+ current (I_{to}) is frequently altered in cardiac disease models (40–42). Therefore, we sought to determine whether changes in I_{to} contributed to APD shortening in $Cdon^{-/-}$ hearts. $Cdon^{-/-}$ myocytes exhibited significantly increased I_{to}, compared with WT controls (*SI Appendix*, Fig. 8 *C* and *D*). The densities of inward rectifier (I_{K1}) and sustained current (I_{sus}) were slightly reduced in $Cdon^{-/-}$ myocytes. To investigate the molecular basis for changes in I_{to}, we examined levels of the α-subunit (Kv4.3 and Kv4.2) and β-subunit (KChIP2) underlying this current. KChIP2 expression

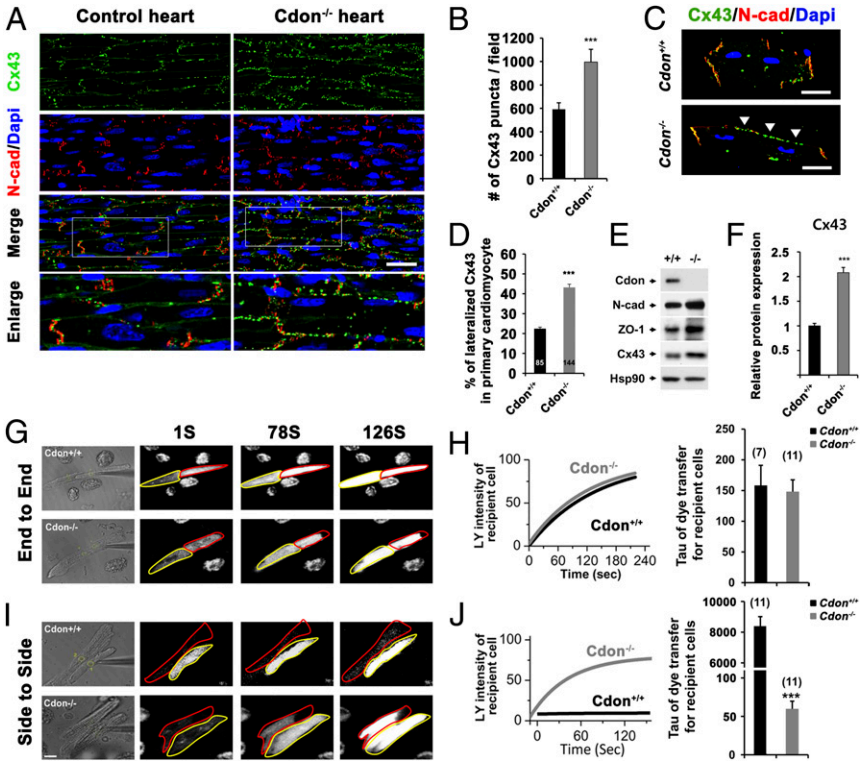

Fig. 4. Cdon deficiency causes alterations in Cx43 levels and localization. (*A*) Immunostaining of $Cdon^{+/+}$ and $Cdon^{-/-}$ hearts for Cx43 (green) and N-cad (red) as a marker of the ID. (Scale bar, 50 μm.) Boxed areas are enlarged in the *Lower* panels. (*B*) Quantificational analysis for Cx43 puncta in *A*. (n = 6) ***P = 0.005. (*C*) Representative immunostaining images of isolated $Cdon^{+/+}$ or $Cdon^{-/-}$ primary cardiomyocytes for Cx43 and N-cad. (Scale bar, 20 μm.) Arrowheads indicate lateralized Cx43. (*D*) Quantification of lateralized Cx43 in *C*. n = 85 for $Cdon^{+/+}$, n = 144 for $Cdon^{-/-}$ cells. ***P < 0.001. (*E* and *F*) Western blot analysis for the expression of cardiac intercalated disc proteins in $Cdon^{+/+}$ and $Cdon^{-/-}$ hearts. HSP90 was used as a loading control. $Cdon^{-/-}$ hearts exhibit twofold increased Cx43 protein level compared with control heart. ***P < 0.005. n = 3. (*G*–*J*, *Left*) Measurement of Lucifer yellow (LY) dye flux in end-to-end (*G*) or side-to-side cell pairs (*I*) and subsequent LY dye transfer from a single injected cell to a recipient cell in $Cdon^{+/+}$ and $Cdon^{-/-}$ cardiomyocytes at 1, 78, and 126 s. Donor cells and recipient cells were marked with a yellow or red line, respectively. Representative regions of interest used to quantify the LY fluorescence are shown in the phase contrast image. (*H* and *J*) Representative fitted single time courses of light intensity in recipient cell from cell pairs and summarized τ data of LY transfer in recipient cell from each cell pair shown in *G* and *I*, respectively. Note that the time constant (τ, time to reach ~63% peak) for end-to-end coupling was 158.28 ± 32.70 (n = 7) in WT and 146.6 ± 38.86 (n = 11) in $Cdon^{-/-}$ myocytes (NS). τ for the side-to-side coupling, which was 6,957 ± 997.27 (n = 11) in WT, significantly reduced to 56.60 ± 5.0 in $Cdon^{-/-}$ myocytes (n = 11, ***P < 0.005). [Scale bar (*Lower Left*) 20 μm.] All experiments in this figure were repeated three times with similar results.

was greatly enhanced in *Cdon*$^{-/-}$ hearts, compared with WT, whereas others were unchanged (*SI Appendix*, Fig. 8*E*). Thus, increased I_{to} levels in *Cdon*$^{-/-}$ myocytes are likely the underlying mechanism for APD shortening. In contrast, calcium cycling or contractile proteins (Serca2a, RyR2, NCX, Cav1.2, and CaM) are not significantly affected (*SI Appendix*, Fig. 9 *A* and *B*). Collectively, these data suggest that not only conduction abnormality but also significant remodeling of the major outward K^+ currents might contribute to incidence of arrhythmias in *Cdon*$^{-/-}$ mice.

Cdon Depletion Induces Gap Junction Remodeling in Primary Rat Cardiomyocytes. To confirm the in vivo data, NRVM cells were transfected with expression vectors for control pSuper or *Cdon*-shRNA and assessed for Cx43 regulation. In agreement with the data from *Cdon*$^{-/-}$ cardiomyocytes, the partial *Cdon* knockdown in NRVM cells resulted in up-regulation of cell surface resident Cx43 to roughly 1.8-fold relative to control-shRNA cells (Fig. 5*A*). The immunostaining of control or Cdon-knockdown cardiomyocytes for Cx43 and N-cadherin and quantification analysis revealed that Cdon knockdown increased the size and number of Cx43 puncta at the cell border (Fig. 5*B*). Then we have examined the functional consequence of Cx43 up-regulation by LY transfer (Fig. 5*C*). After injection into a centrally situated myocyte (marked with a yellow line), the number of fluorescent cells was significantly increased in Cdon-knockdown cells, which was recovered to control level by Cdon reexpression (Fig. 5*D*). These data further suggest that Cdon deficiency results in up-regulation of Cx43 gap junction.

Cdon Regulates Gap Junction Activity via Suppression of Wnt/β-Catenin Signaling. Considering that Wnt/β-catenin signaling is reactivated by pathological stress, contributing to cardiac remodeling and fibrosis (11), we have assessed the cross-talk between Cdon and Wnt signaling in cardiomyocytes. About 18% of Cdon-depleted NRVM cells exhibited nuclear β-catenin accumulation, compared with 2% of the control-transfected cells (Fig. 6*A* and *SI Appendix*, Fig. 10), suggesting elevated Wnt signaling activation in Cdon-knockdown cells. Consistently, the immunoblot analysis of 2-wk-old control and *Cdon*$^{-/-}$ hearts shows that the level of the inactive phosphorylated form of GSK3β (p-GSK3β), an inhibitory component of Wnt signaling through promoting β-catenin degradation, was markedly increased in *Cdon*$^{-/-}$ heart lysates, compared with the control hearts. Total β-catenin and phosphorylated LRP6 (p-LRP6) levels were significantly elevated in *Cdon*$^{-/-}$ heart, relative to the controls (Fig. 6 *B* and *C*). These data suggest that hyperactivated Wnt signaling likely contributes to cardiac fibrosis and remodeling observed in *Cdon*$^{-/-}$ hearts.

To further assess the cross-talk between Wnt signaling and Cdon, NRVM cells were treated with a Wnt signaling agonist TWS119 (0.8 μM) for 24 h and subjected to immunoblotting (Fig. 6*D*). As expected, TWS119 treatment enhanced Wnt signaling activities as observed by elevated levels of the active phosphorylated form of Wnt coreceptor LRP6 (p-LRP6) and p-GSK3β without altered total protein levels. It is of note that Cdon protein levels decreased substantially with the TWS119 treatment. Similar to Cdon-depleted myocytes, TWS119-treated cells exhibited roughly 1.8-fold up-regulated cell surface-resident Cx43 proteins compared with the vehicle-treated cells (Fig. 6*E*). This elevation of surface Cx43 proteins led to a fourfold increase in LY dye transfer ($P < 0.01$) (Fig. 6 *F* and *G*). Next, we examined whether a Wnt inhibitor, XAV939 (4 μM for 24 h) treatment prevented collagen accumulation and Cx43 up-regulation caused by Cdon deficiency. Cdon depletion in NRVMs led to enhanced Axin2 expression about threefold relative to the control transfected cells, which was significantly decreased by XAV939 treatment (Fig. 6*H*). XAV939 treatment reduced Collagen1 levels equivalent to control (Fig. 6*I*). We also confirmed that LY dye transfer and Cx43 puncta size in Cdon-knockdown cells returned to control levels by inhibition of Wnt signaling with other inhibitors Dkk1 (20 ng/mL for 24 h, Fig. 6 *J* and *K*) and IWP2 (2 μM for 24 h, Fig. 6 *L*–*O*). In contrast, the treatment with Shh or transforming growth factor (TGF)-β had no effect on LY dye transfer in control and Cdon-knockdown cells (*SI Appendix*, Fig. 11 *A* and *B*). In addition, the expression of TGF-β and endogenous Wnt signaling inhibitors, DKK1, DKK2, DKK3, secreted frizzled related protein 1 (sFRP1), and sFRP2, was not significantly changed in Cdon-deficient hearts (*SI Appendix*, Fig. 11*C*). These data demonstrate that inhibition of Wnt signaling restores aberrant gap junction activity in *Cdon*-depleted cardiomyocytes.

Dysregulated cell-to-cell coupling can give rise to ectopic activation and local propagation delays, disturbing synchronized conduction (43, 44). To assess the conduction properties, we have performed optical mapping analysis using monolayers of control and Cdon-knockdown cardiomyocytes (*SI Appendix*, Fig. 12 *A* and *B*). The conduction velocity (CV) was significantly lower in Cdon-knockdown NRVM cells ($P < 0.005$ vs. control, $P < 0.05$ vs. control pSuper). Slow conduction also led to

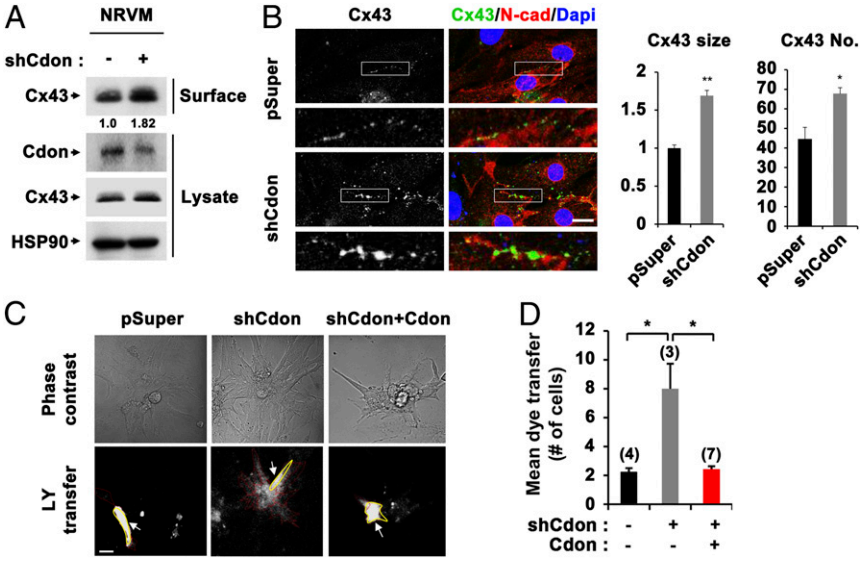

Fig. 5. Increased surface localization of Cx43 and aberrant gap junction activity was induced by Cdon depletion in NRVM cells. (*A*) Biotinylation of NRVM cells with control or shCdon transfection. (*B*) Representative confocal images for Cx43 and N-cad in control and shCdon NRVM cells. The quantification of Cx43 sizes and numbers are shown in *Middle* and *Right* panels, respectively. *$P < 0.05$, **$P < 0.01$. (Scale bar, 10 μm.) (*C*) Measurement of LY flux for 5 min postinjection in rat cardiac cells transfected with control pSuper, shCdon alone, or shCdon with Cdon. (Scale bar, 20 μm.) Donor cells and recipient cells were marked with yellow (indicated with arrow) or red line, respectively. (*D*) Quantification of cell numbers for mean dye transfer. Numbers in bars indicate numbers of experiments in each group. *$P < 0.05$.

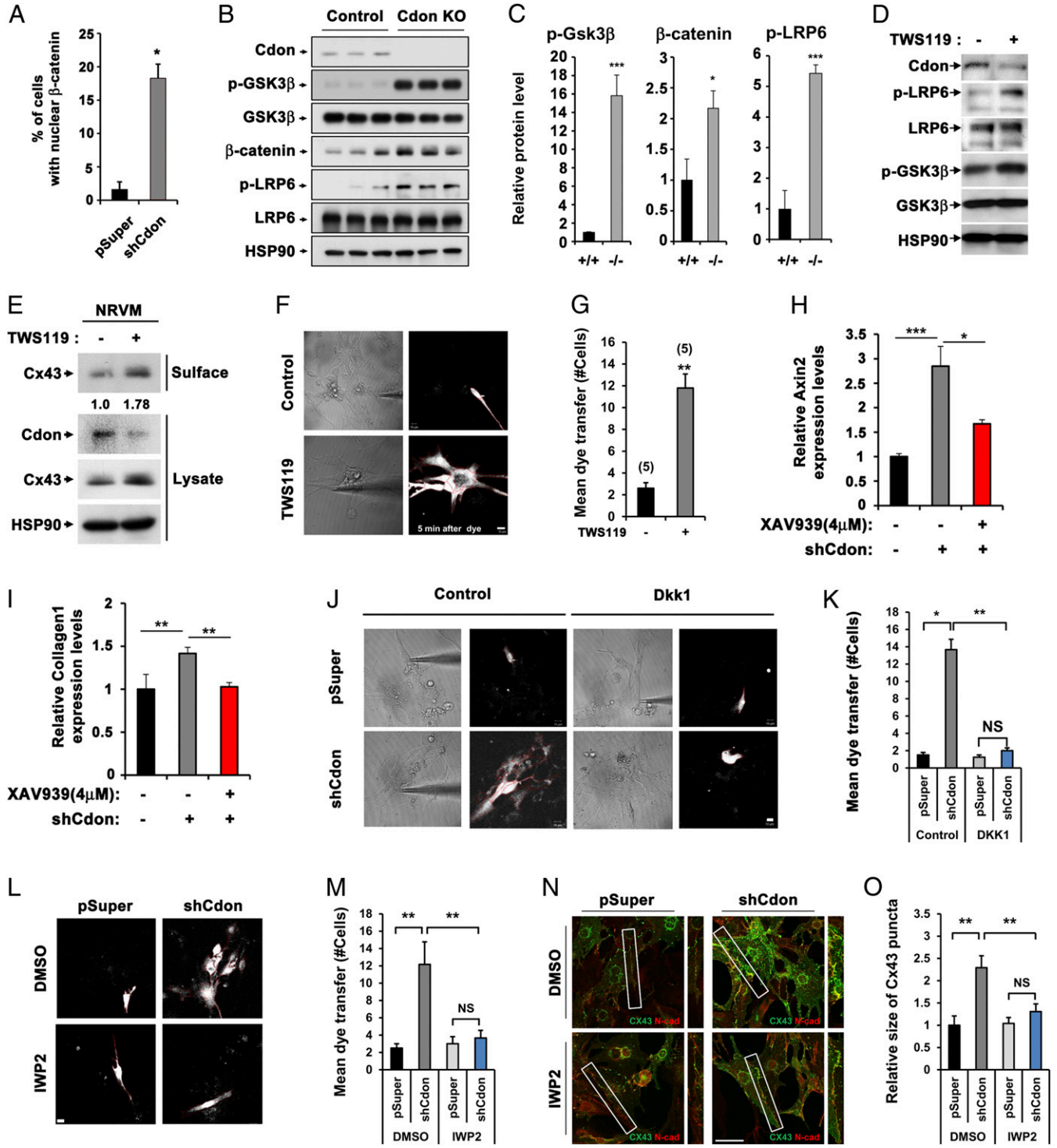

Fig. 6. Reciprocal actions of Wnt and Cdon on gap junction activity. (*A*) Quantification of the nuclear β-catenin accumulation in control ($n = 131$) and Cdon KD NRVM cells ($n = 110$). $^*P < 0.05$. (*B*) Western blot analysis of heart lysate from control and Cdon KO mice at postnatal day 14 for protein expression of Cdon, p-GSK3β, GSK3β, β-catenin, p-LRP6, and LRP6. HSP90 was used as loading control. (*C*) Quantificational analysis of the relative levels of p-GSK3β/GSK3β, β-catenin, and p-LRP6/LRP6 proteins in *B*. $^*P < 0.05$, $^{***}P < 0.005$. (*D*) Immunoblot analysis of cell lysates from rat cardiac cells treated with 0.8 μM of TWS119 or the vehicle DMSO for 24 h. The experiments shown in this figure are repeated at least twice with similar results. (*E*) Immunoblotting of biotinylation of NRVM cells treated with control DMSO or 0.8 μM TWS119. (*F*) Measurement of LY flux for 5 min postinjection in NRVM cells treated with 0.8 μM TWS119 or vehicle DMSO for 24 h. (Scale bar, 10 μm.) (*G*) Quantificational data from *F*. Numbers in bars indicate numbers of experiments in each group. $^{**}P < 0.01$. (*H* and *I*) qPCR analysis for Axin2 and Collagen 1 expression in control or shCdon transfected NRVM cells treated with 4 μM of XAV939 or vehicle DMSO. $^*P < 0.05$, $^{**}P < 0.01$, $^{***}P < 0.005$. $n = 3$. (*J* and *L*) Measurement of LY flux for NRVM cells with the transfection of control or shCdon in combination with the treatment of Wnt inhibitor Dkk1 or control medium (*J*) and IWP2 or control DMSO (*L*). (Scale bar, 10 μm.) (*K* and *M*) Quantification of cell numbers for mean dye transfer for *J* and *L*, respectively. Numbers in bars indicate numbers of experiments in each group. $^*P < 0.05$, $^{**}P < 0.01$. NS, no significance. (*N*) Immunostaining of NRVM cells for the localization of Cx43 (green) and N-cadherin (red). (Scale bar, 20 μm.) (*O*) Quantification data for size of Cx43 puncta from *N*. $^{**}P < 0.01$. NS, no significance. $n = 15$.

shortening of voltage wavelength. Furthermore, the propagation was not even in monolayer Cdon-knockdown cells, due to formation of heterogeneous regions with low excitability (see Movie S1 for control, Movie S2 for pSuper, and Movie S3 for shCdon). In some monolayers of Cdon-depleted cells, spontaneous activity was also observed (Movie S4). All these factors can increase arrhythmogenic potentials. Thus, Cdon deficiency induces a disruption of impulse propagation, contributing to cardiac arrhythmias in *Cdon*$^{-/-}$ mice. In conclusion, these data demonstrate that Cdon deficiency causes hyperactivation of Wnt signaling in cardiomyocytes, which in turn induces fibrosis and gap junction remodeling, leading to cardiac arrhythmias and cardiomyopathy.

Discussion

Considering that Wnt signaling is reactivated after cardiac injury and its involvement in cardiac fibrosis and hypertrophy (45, 46), modulation of Wnt signaling represents a beneficial target to intervene in cardiac diseases. Consistently, inhibition of reactivated Wnt signaling has been shown to attenuate the hypertrophic responses (12–14). Although much has been studied about the role of Wnt signaling in cardiac hypertrophy and infarction, the regulatory mechanisms of Wnt signaling in cardiac remodeling is not fully understood. The current study demonstrates a critical role of Cdon in the maintenance of intercellular coupling and cardiac function. Cdon deficiency induces hyperactivation of Wnt/β-catenin signaling, which might contribute to the signal transduction of structural remodeling, leading to up-regulation and lateralization of Cx43, and cardiac fibrosis. Our reasons to support the role of Wnt signaling in the cardiac remodeling of *Cdon*$^{-/-}$ mice are threefold. First, fibrosis and structural remodeling in *Cdon*$^{-/-}$ hearts were accompanied by alterations in global gene expression, including genes involved in cardiac remodeling, linked with Wnt signaling (11, 47). Second, *Cdon*$^{-/-}$ mice exhibited hyperactivation of Wnt signaling as evident by accumulation of β-catenin, up-regulation of Axin2, a target of Wnt signaling and inhibition of GSK3β, a negative regulator of Wnt signaling (48). Third, an inhibition of Wnt signaling in Cdon-depleted cardiomyocytes restored intercellular coupling and collagen expression to the control level. Thus, current study suggests that Cdon is essential to keep Wnt signaling under physiological level, thereby preventing abnormal myocardial structure and conduction.

The cardiac remodeling process is governed by structural and electrical changes that decrease the electrical stability of the heart. A hallmark of the electrical changes with regard to impulse conduction is a change in electrical coupling due to abnormal expression of Cx43-constituted gap junctions. Cx43 localization is regulated through a variety of mechanisms, including protein trafficking following translation and overall stabilization of intercalated discs. Recently the role of Wnt in expression of Cx43 has been established (24, 49). Consistently, we confirmed that Wnt inhibitor reversed up-regulation of Cx43 level and cell–cell coupling in Cdon-knockdown neonatal cardiomyocytes. Thus, Cx43 remodeling in Cdon-deficient cardiomyocytes might be at least partially attributable to Wnt signaling. However, due to limitation of neonatal cardiomyocytes, the underlying mechanism of Cdon-deficiency–induced Cx43 lateralization cannot be investigated. Neonatal myocytes are more rounded, with no anisotropy of structure, unlike the elongated adult myocyte alignment in anisotropic tissue. Cx43 in cultured neonatal myocytes (as in intact neonatal ventricular myocardium) is distributed around the entire cell perimeter rather than being located at the poles of the cells in IDs in adult myocytes (50–52). It is plausible that Cdon might regulate the localization of Cx43 through a Wnt-independent pathway, such as N-cadherin or LRP6, because Cdon is localized at the ID and directly interacts with N-cadherin (53) and LRP6 (28), both of which are implicated in proper localization of Cx43 (54–57). Regardless, the results presented here provide direct evidence of a functional role for Cdon in the control of Cx43 expression and its localization to the ID at the site of end-to-end contacts between cardiomyocytes.

The major adverse effects of Cdon deletion in the mouse myocardium are an increase of fibrosis and dysregulation of gap junction, and both of them can disrupt the impulse conduction. Consistently, optical mapping data showed the delay of conduction and the formation of heterogeneous regions with low excitability, which may critically heighten the risk of lethal arrhythmia (58). We confirmed that *Cdon*$^{-/-}$ mice showed spontaneous arrhythmias, including complete AV block and PVC that might develop ventricular tachycardia or ventricular fibrillation. Hence, in *Cdon*$^{-/-}$ hearts the electrical remodeling and arrhythmias can be based on the disruption of impulse conduction.

Activation of Wnt signaling by treatment with a Wnt agonist TWS119 in neonatal cardiomyocytes markedly enhances collagen and Cx43 expression, whereas it represses Cdon levels, suggestive of a feedback mechanism. Previously, a feedback mechanism between Cx43 and β-catenin has been proposed to modulate intercellular coupling of cardiomyocytes (59). Together, our data suggest that Cdon might be involved in a feedback mechanism to suppress Wnt signaling in normal cardiac function. Considering that Cdon was one of the genes decreased in humans with dilated cardiomyopathy (accession: GDS2206, ID: 2206), the reduction of Cdon may shift the balance between Cdon and Wnt signal toward cardiac remodeling. The suppressive activity of Wnt signaling by Cdon can be an attractive mechanism as a target for the prognosis and intervention of cardiomyopathy and fibrosis.

Methods

Mice. *Cdon*$^{+/-}$ mice were maintained as previously described (25, 27). Briefly, *Cdon*$^{+/-}$ mice were kept on a C57BL/6 background and 2- or 3-mo-old mice were used for breeding. From heterozygous crosses, wild-type or heterozygous littermates were used as controls for the phenotypic studies of *Cdon*$^{-/-}$ mice. This study was reviewed and carried out in accordance with the Institutional Animal Care and Use Committee of Sungkyunkwan University School of Medicine (SUSM). SUSM is an Association for Assessment and Accreditation of Laboratory Animal Care International accredited facility and abides by the Institute of Laboratory Animal Resources Guide.

Isolation of Mouse Ventricular Myocytes and Microinjection of Lucifer Yellow. To isolate ventricular myocytes, 2-wk-old *Cdon*$^{+/+}$ and *Cdon*$^{-/-}$ littermates were used. Ventricular myocytes were isolated by perfusion with a Ca^{2+}-free normal Tyrode solution containing collagenase (Worthington, type 2) on a Langendorff column at 37 °C as previously described (60) with minor modifications. Isolated ventricular myocytes were kept in high K^+, low Cl^- solution at 4 °C until use. Normal Tyrode solution contained (in millimoles per liter) 140 NaCl, 5 KCl, 1 $MgCl_2$, 1.8 $CaCl_2$, 10 Hepes, and 10 glucose, adjusted to pH 7.4 with NaOH. The Ca^{2+}-free solution contained (in millimoles per liter) 140 NaCl, 5 KCl, 1 $MgCl_2$, 10 Hepes, and 10 glucose, adjusted to pH 7.4 with NaOH. The high K^+, low Cl^- solution contained (in millimoles per liter) only Ca^{2+}-tolerant, rod-shaped myocytes with cross-striations and without spontaneous contractions or significant granulation were selected for electrophysiological experiments.

LY dye transfer through gap junction channels was investigated using cell pairs. LY (Molecular Probes) was dissolved in the pipette solution to reach a concentration of 2 mmol/L (61). A micropipette (tip resistance 2.5 ± 0.5 MΩ) was used to inject LY into myocytes; after a gigaohm seal was established, the cell membrane at the tip of the pipette was ruptured by applying brief suction. Microinjection and image recording were performed using confocal microscopy (Carl Zeiss).

Newborn Rat Cardiomyocyte Isolation and Transfection. Cardiac myocytes were isolated from neonatal Sprague-Dawley (1–2 d) rat hearts by using a previously reported method (62). Ventricular tissues (~1–2 mm) were excised and minced on ice. The minced tissues were treated with a solution containing 0.1% collagenase (Worthington, type 2), 0.1% trypsin, and 1% glucose in PBS (Ca^{2+}/Mg^{2+}-free) at 37 °C for 10 min. After the supernatant

from the first digestion was removed, three 10-min digestions were performed using the same enzyme solution. The supernatants were stored in DMEM/F-12 culture medium containing 10% (vol/vol) FBS, 5% (vol/vol) horse serum, penicillin–streptomycin (100 units/mL and 100 μg/mL, respectively) in a 4 °C ice chamber and centrifuged for 7 min at 700 × *g*. The cell pellets were incubated at 37 °C in a 95% (vol/vol) O_2 incubator for 1.5 h to remove noncardiac myocytes by attachment on coverglass. The remaining cells were subsequently cultured on the coverglass for 3 d at 37 °C and 95% (vol/vol) O_2. To analyze the function of Cdon in gap junctional communication, isolated rat cardiac cells were transfected with the combination of shRNA-Cdon, pBP-Cdon (29) by Lipofectamine 2000 reagent followed by 48 h of culture incubation. Additional XAV939 (4 μM, Calbiochem), IWP2 (2 μM, Calbiochem), Dkk1(20 ng/mL, Merck Millipore), Shh (250 ng/mL, R&D System), and human TGF-β (2 ng/mL, R&D System) were treated for 24 h before the LY dye transfer assay.

Antibodies and Immunoblotting. The primary antibodies used for immunostaining include α-actinin (Sigma-Aldrich; 1:250), β-catenin (BD Biosciences; 1:250), Cdon (R&D Systems; 1:50), connexin 43 (Cx43, Cell Signaling; 1:250), DDR2 (Santa Cruz; 1:250), N-cadherin (Abcam; 1:1,000), and Zonula Occludens-1 (ZO-1, Invitrogen; 1:250). The antibodies used for immunoblotting include β-tubulin, p-S368 Cx43, Cx43, GSK3β, pGSK3β, LRP6, p-LRP6, t-RYR2, and p-RYR2 (Cell Signaling; 1:1,000), α-actinin (1:1,000), α-catenin (Abcam; 1:10,000), Cdon (R&D Systems; 1:1,000), cTnT, α-SMA, and N-cadherin (Abcam; 1:1,000), CaV1.2 (Alomone Labs; 1:1,000), Kchip2 (Thermo Scientific; 1:1,000), Kv4.2 and Kv4.3 (Millipore; 1:1,000), β-catenin, CaM, DDR2, HSP90, and NCX (Santa Cruz; 1:1,000), Serca2a (Pierce; 1:1,000), and ZO-1 (Invitrogen; 1:1,000).

Western blot analyses were performed as described previously (63). Briefly, lysed heart tissues or freshly isolated cardiac cells were subjected to SDS/PAGE and immunoblotting, using various primary antibodies. Transferred membranes were blocked with 5% (wt/vol) skim milk in TBST (10 mM Tris–HCl, pH 8.0, 150 mM NaCl, 0.1% Tween-20) for 30 min and incubated with the primary antibodies at 4 °C overnight.

Biotinylation of NRVM cells was performed as described previously (31). Briefly, control and Cdon KD- or TWS119-treated NRVM cells were incubated with PBS containing sulfo-NHS-LC-biotin (1 mg/mL) for 30 min on ice followed by two cold PBS washes. After quenching the biotinylation with 100 mM glycine in PBS, cells were sonicated and lysed in cell lysis buffer. Biotinylated proteins were pulled down with streptavidin agarose beads and analyzed with SDS/PAGE.

Tissue Preparation, Histology, and Immunostaining. Histology and immunostaining of heart sections was performed as previously described (64). Briefly, dissected hearts from animals were fixed in 4% (wt/vol) paraformaldehyde and embedded into OCT or paraffin blocks. Paraffin-embedded tissues were sliced with 4-μm thickness and stained with hematoxylin and eosin (H&E), or Masson's trichrome. For immunostaining, frozen tissues were sliced with 7-μm thickness and primary antibodies diluted 1:250 in 5% (vol/vol) goat serum or 2% (wt/vol) BSA in 0.15% PBST buffer followed by serial rehydration and antigen retrieval with 20 μg/mL of proteinase K (Roche) incubation. Images were analyzed with an LSM-710 confocal microscope system (Carl Zeiss) or Nikon ECLIPS TE-2000U and NIS-Elements F software (Nikon). For isolated single primary cardiomyocytes, cells were plated on laminin-coated coverslips and incubated for 3 h at 4 °C in Krebs-Henseleit buffer, gently washed in 0.01 M PBS, then fixed with 4% (wt/vol) paraformaldehyde at room temperature for 30 min. Plated cells were washed three times and permeabilized with 0.2% Triton X-100 containing 0.1 M glycine (Sigma), then blocked with 10% (vol/vol) goat serum in PBS for 30 min. Cells were incubated overnight with primary antibodies diluted in blocking buffer. Primary and secondary antibodies were diluted at 1:250 or 1:500 in blocking solution overnight at 4 °C or 1 h at room temperature, respectively. The signal intensities of Cdon, Cx43, and N-cadherin in ID areas were measured by ZEN microscope software (Carl Zeiss). Quantification of lateralized Cx43 was assessed by IN Cell Analyzer 2200 (GE Healthcare Life Sciences). To obtain normal human atrial tissue, written informed consent was provided before surgery. The patient had aortic valve disease with normal atrial function who was requiring the aortic valve replacement. Before aortic valve replacement, we obtained the left atrial tissue from the left atrial appendage using a surgical stapler. For the immunostaining, tissue was processed for frozen section similarly to mouse tissues. To examine the cell death in control and Cdon KO mouse hearts, TUNEL imaging assays (Click-iT TUNEL Alexa Fluor Imaging Assay) were performed according to the manufacturer's instructions.

RNA Analysis. Total RNA from hearts of neonatal *Cdon*$^{+/+}$ and *Cdon*$^{-/-}$ littermates was isolated with easy-BLUE reagent (Intron Biotechnology) following manufacturer's instructions. For RNA sequencing analysis, total RNA was isolated using TRIzol reagent (Invitrogen). RNA quality was assessed by Agilent 2100 bioanalyzer using the RNA 6000 Nano Chip (Agilent Technologies), and RNA quantification was performed using ND-2000 Spectrophotometer (Thermo Scientific). For control and sample RNAs, the construction of a library was performed using SENSE 3′ mRNA-Seq Library Prep Kit (Lexogen) according to the manufacturer's instructions. High-throughput sequencing was performed as single-end 75 sequencing using NextSEq. 500 (Illumina). For data analysis, SENSE 3′ mRNA-Seq reads were aligned using Bowtie2 version 2.1.0 (65). Bowtie2 indices were either generated from genome assembly sequence or the representative transcript sequences for aligning to the genome and transcriptome. The alignment file was used for assembling transcripts, estimating their abundances and detecting differential expression of genes. Differentially expressed genes were determined based on counts from unique and multiple alignments using EdgeR within R version 3.2.2 (R Development Core Team, 2011) using BIOCONDUCTOR version 3.0 (66). The RT (read count) data were processed based on the quantile normalization method using Genowiz version 4.0.5.6 (Ocimum Biosolutions).

For quantitative RT-PCR, cDNA samples were made from 0.5 μg of total RNA with the PrimeScript RT reagent kit (TaKaRa) according to the manufacturer's instructions. Quantitative RT-PCR was performed with SYBR premix Ex taq (TaKaRa) using the Thermal Cycler Dice Real Time system analysis. The primer sequences used in this study are shown in *SI Appendix*, Table 4.

Electrophysiology. Membrane currents were recorded from single isolated myocytes in a perforated patch configuration by using nystatin (200 μg/mL; ICN) at 35 ± 1 °C. Voltage clamp was performed by using an EPC-10 amplifier (HEKA Instruments) and filtered at 10 kHz. The pipette solution for perforated patches contained (in millimoles): KCl 140, Hepes 10, $MgCl_2$ 1, EGTA 5, titrated to pH 7.2 with KOH. The patch pipettes (World Precision Instruments) were made by a Narishige puller (PP-830; Narishige). The patch pipettes used had a resistance of 2–3 MΩ when filled with the below pipette solutions. All recordings were carried out at room temperature.

Echocardiography and Electrocardiogram. M-mode echocardiography was performed on 2-wk-old wild-type and *Cdon*-knockout mice under 1–2% (vol/vol) isoflurane anesthesia using a Visual Sonics Vevo 2100 system equipped with a 40-MHz probe (Visual Sonics). The internal LV end-diastolic and end-systolic dimensions (LVID;d and LVID;s) were measured in the short axis view at the level of the papillary muscles. The fractional shortening (%FS) was calculated using the equation %FS = [(LVID;d − LVID;s)/LVID;d] × 100 and ejection fraction (EF) using the equation: [(LVV;d − LVV;s)/LVV;d] × 100, where LVV;d and LVV;s represent LV volume; end diastolic and end systolic.

To record the electrocardiogram, mice were anesthesized with 2% (vol/vol) isoflurane, placed in the prone position on a warm surface essentially as previously published (67). A Lead II ECG was recorded with s.c. electrodes using a PowerLab station (AD Instruments) and LabChart7 software. Heart rate and QRS interval duration were determined by averaging three consecutive beats during sinus rhythm.

Optical Mapping Analysis. Confluent monolayers of NRVMs were stained with 5 μmol/L di-4-ANEPPS (voltage sensitive fluorescent dye) for ∼30 min after 24∼48 h of transfection of control shRNA or Cdon-shRNA. They were then washed, put in the chamber of the optical mapping setup, superfused with Tyrode's solution consisting of (in millimoles per liter) 135 NaCl, 5.4 KCl, 1.8 CaCl2, 1 MgCl2, 0.33 NaH_2PO_4, 5 Hepes, and 5 glucose and maintained at 31 °C. The monolayer was paced with voltage pulses of 1 Hz. Software written in MATLAB and LabVIEW was used to record the changes in cellular membrane voltage and analyze the propagation of voltage wave through each monolayer.

Statistical Analysis. Values are means ± SEM or SD as noted. Statistical significance was calculated by paired or unpaired two-tailed Student's *t* test; differences were considered significant at $P < 0.05$.

ACKNOWLEDGMENTS. We thank Drs. Ruth Simon and Won-Kyung Ho for critical discussion and reading of the manuscript. This research was supported by the Bio and Medical Technology Development Program of National Research Foundation (NRF) funded by the Korean Government, Grants NRF-2015R1A2A1A15051998 and NRF-2016R1A2B2007179.

1. Bui AL, Horwich TB, Fonarow GC (2011) Epidemiology and risk profile of heart failure. *Nat Rev Cardiol* 8(1):30–41.
2. Katz AM (1990) Cardiomyopathy of overload. A major determinant of prognosis in congestive heart failure. *N Engl J Med* 322(2):100–110.
3. Mozaffarian D, et al.; American Heart Association Statistics Committee and Stroke Statistics Subcommittee (2015) Heart disease and stroke statistics–2015 update: A report from the American Heart Association. *Circulation* 131(4):e29–e322.
4. Creemers EE, Pinto YM (2011) Molecular mechanisms that control interstitial fibrosis in the pressure-overloaded heart. *Cardiovasc Res* 89(2):265–272.
5. Flesch M, et al. (1996) Sarcoplasmic reticulum Ca2+ATPase and phospholamban mRNA and protein levels in end-stage heart failure due to ischemic or dilated cardiomyopathy. *J Mol Med (Berl)* 74(6):321–332.
6. Jiang DS, et al. (2014) IRF8 suppresses pathological cardiac remodelling by inhibiting calcineurin signalling. *Nat Commun* 5:3303.
7. Jiang X, et al. (2015) Tumor necrosis factor receptor-associated factor 3 is a positive regulator of pathological cardiac hypertrophy. *Hypertension* 66(2):356–367.
8. Komiya Y, Habas R (2008) Wnt signal transduction pathways. *Organogenesis* 4(2): 68–75.
9. MacDonald BT, Tamai K, He X (2009) Wnt/beta-catenin signaling: Components, mechanisms, and diseases. *Dev Cell* 17(1):9–26.
10. Tian Y, Cohen ED, Morrisey EE (2010) The importance of Wnt signaling in cardiovascular development. *Pediatr Cardiol* 31(3):342–348.
11. Bergmann MW (2010) WNT signaling in adult cardiac hypertrophy and remodeling: Lessons learned from cardiac development. *Circ Res* 107(10):1198–1208.
12. Zelarayán LC, et al. (2008) Beta-Catenin downregulation attenuates ischemic cardiac remodeling through enhanced resident precursor cell differentiation. *Proc Natl Acad Sci USA* 105(50):19762–19767.
13. Baurand A, et al. (2007) Beta-catenin downregulation is required for adaptive cardiac remodeling. *Circ Res* 100(9):1353–1362.
14. Zhou J, et al. (2007) Upregulation of gamma-catenin compensates for the loss of beta-catenin in adult cardiomyocytes. *Am J Physiol Heart Circ Physiol* 292(1):H270–H276.
15. Kaplan SR, et al. (2004) Remodeling of myocyte gap junctions in arrhythmogenic right ventricular cardiomyopathy due to a deletion in plakoglobin (Naxos disease). *Heart Rhythm* 1(1):3–11.
16. Luke RA, Saffitz JE (1991) Remodeling of ventricular conduction pathways in healed canine infarct border zones. *J Clin Invest* 87(5):1594–1602.
17. Beardslee MA, et al. (2000) Dephosphorylation and intracellular redistribution of ventricular connexin43 during electrical uncoupling induced by ischemia. *Circ Res* 87(8):656–662.
18. Akar FG, et al. (2007) Dynamic changes in conduction velocity and gap junction properties during development of pacing-induced heart failure. *Am J Physiol Heart Circ Physiol* 293(2):H1223–H1230.
19. Smith JH, Green CR, Peters NS, Rothery S, Severs NJ (1991) Altered patterns of gap junction distribution in ischemic heart disease. An immunohistochemical study of human myocardium using laser scanning confocal microscopy. *Am J Pathol* 139(4): 801–821.
20. Li J, et al. (2012) Loss of αT-catenin alters the hybrid adhering junctions in the heart and leads to dilated cardiomyopathy and ventricular arrhythmia following acute ischemia. *J Cell Sci* 125(Pt 4):1058–1067.
21. Pieperhoff S, Franke WW (2007) The area composita of adhering junctions connecting heart muscle cells of vertebrates - IV: Coalescence and amalgamation of desmosomal and adhaerens junction components - late processes in mammalian heart development. *Eur J Cell Biol* 86(7):377–391.
22. Severs NJ, Bruce AF, Dupont E, Rothery S (2008) Remodelling of gap junctions and connexin expression in diseased myocardium. *Cardiovasc Res* 80(1):9–19.
23. Teunissen TA, van den Bosch WJ, van den Hoogen HJ, Lagro-Janssen AL (2004) Prevalence of urinary, fecal and double incontinence in the elderly living at home. *Int Urogynecol J Pelvic Floor Dysfunct* 15(1):10–13, discussion 13.
24. van der Heyden MA, et al. (1998) Identification of connexin43 as a functional target for Wnt signalling. *J Cell Sci* 111(Pt 12):1741–1749.
25. Zhang W, et al. (2006) Cortical thinning and hydrocephalus in mice lacking the immunoglobulin superfamily member CDO. *Mol Cell Biol* 26(10):3764–3772.
26. Zhang W, Kang JS, Cole F, Yi MJ, Krauss RS (2006) Cdo functions at multiple points in the Sonic Hedgehog pathway, and Cdo-deficient mice accurately model human holoprosencephaly. *Dev Cell* 10(5):657–665.
27. Cole F, Zhang W, Geyra A, Kang JS, Krauss RS (2004) Positive regulation of myogenic bHLH factors and skeletal muscle development by the cell surface receptor CDO. *Dev Cell* 7(6):843–854.
28. Jeong MH, et al. (2014) Cdo suppresses canonical Wnt signalling via interaction with Lrp6 thereby promoting neuronal differentiation. *Nat Commun* 5:5455.
29. Lu M, Krauss RS (2010) N-cadherin ligation, but not Sonic hedgehog binding, initiates Cdo-dependent p38alpha/beta MAPK signaling in skeletal myoblasts. *Proc Natl Acad Sci USA* 107(9):4212–4217.
30. Feranchak AP, et al. (2010) Initiation of purinergic signaling by exocytosis of ATP-containing vesicles in liver epithelium. *J Biol Chem* 285(11):8138–8147.
31. Yoo M, et al. (2015) Syntaxin 4 regulates the surface localization of a promyogenic receptor Cdo thereby promoting myogenic differentiation. *Skelet Muscle* 5:28.
32. Nosi D, et al. (2013) A molecular imaging analysis of Cx43 association with Cdo during skeletal myoblast differentiation. *J Biophotonics* 6(8):612–621.
33. Tran P, et al. (2012) TGF-β-activated kinase 1 (TAK1) and apoptosis signal-regulating kinase 1 (ASK1) interact with the promyogenic receptor Cdo to promote myogenic differentiation via activation of p38MAPK pathway. *J Biol Chem* 287(15): 11602–11615.
34. Jansen JA, et al. (2012) Reduced Cx43 expression triggers increased fibrosis due to enhanced fibroblast activity. *Circ Arrhythm Electrophysiol* 5(2):380–390.
35. Adam O, et al. (2010) Rac1-induced connective tissue growth factor regulates connexin 43 and N-cadherin expression in atrial fibrillation. *J Am Coll Cardiol* 55(5): 469–480.
36. Severs NJ, et al. (2004) Gap junction alterations in human cardiac disease. *Cardiovasc Res* 62(2):368–377.
37. Ai X, Zhao W, Pogwizd SM (2010) Connexin43 knockdown or overexpression modulates cell coupling in control and failing rabbit left ventricular myocytes. *Cardiovasc Res* 85(4):751–762.
38. Kléber AG, Rudy Y (2004) Basic mechanisms of cardiac impulse propagation and associated arrhythmias. *Physiol Rev* 84(2):431–488.
39. Nattel S, Maguy A, Le Bouter S, Yeh YH (2007) Arrhythmogenic ion-channel remodeling in the heart: Heart failure, myocardial infarction, and atrial fibrillation. *Physiol Rev* 87(2):425–456.
40. Petkova-Kirova PS, et al. (2006) Electrical remodeling of cardiac myocytes from mice with heart failure due to the overexpression of tumor necrosis factor-alpha. *Am J Physiol Heart Circ Physiol* 290(5):H2098–H2107.
41. Rose J, et al. (2005) Molecular correlates of altered expression of potassium currents in failing rabbit myocardium. *Am J Physiol Heart Circ Physiol* 288(5):H2077–H2087.
42. Kaprielian R, Sah R, Nguyen T, Wickenden AD, Backx PH (2002) Myocardial infarction in rat eliminates regional heterogeneity of AP profiles, I(to) K(+) currents, and [Ca(2+)](i) transients. *Am J Physiol Heart Circ Physiol* 283(3):H1157–H1168.
43. Weiss JN, Nivala M, Garfinkel A, Qu Z (2011) Alternans and arrhythmias: From cell to heart. *Circ Res* 108(1):98–112.
44. Rutherford SL, Trew ML, Sands GB, LeGrice IJ, Smaill BH (2012) High-resolution 3-dimensional reconstruction of the infarct border zone: Impact of structural remodeling on electrical activation. *Circ Res* 111(3):301–311.
45. Ozhan G, Weidinger G (2015) Wnt/β-catenin signaling in heart regeneration. *Cell Regen (Lond)* 4(1):3.
46. Dawson K, Aflaki M, Nattel S (2013) Role of the Wnt-Frizzled system in cardiac pathophysiology: A rapidly developing, poorly understood area with enormous potential. *J Physiol* 591(6):1409–1432.
47. Mozaffarian D, Ludwig DS (2015) Dietary cholesterol and blood cholesterol concentrations: Reply. *JAMA* 314(19):2084–2085.
48. Soares-Miranda L, Siscovick DS, Psaty BM, Longstreth WT, Jr, Mozaffarian D (2016) Physical activity and risk of coronary heart disease and stroke in older adults: The cardiovascular health study. *Circulation* 133(2):147–155.
49. Ai Z, Fischer A, Spray DC, Brown AM, Fishman GI (2000) Wnt-1 regulation of connexin43 in cardiac myocytes. *J Clin Invest* 105(2):161–171.
50. Peters NS, et al. (1994) Spatiotemporal relation between gap junctions and fascia adherens junctions during postnatal development of human ventricular myocardium. *Circulation* 90(2):713–725.
51. Thomas SP, et al. (2000) Synthetic strands of neonatal mouse cardiac myocytes: structural and electrophysiological properties. *Circ Res* 87(6):467–473.
52. Angst BD, et al. (1997) Dissociated spatial patterning of gap junctions and cell adhesion junctions during postnatal differentiation of ventricular myocardium. *Circ Res* 80(1):88–94.
53. Kang JS, Feinleib JL, Knox S, Ketteringham MA, Krauss RS (2003) Promyogenic members of the Ig and cadherin families associate to positively regulate differentiation. *Proc Natl Acad Sci USA* 100(7):3989–3994.
54. Kostin S, Hein S, Bauer EP, Schaper J (1999) Spatiotemporal development and distribution of intercellular junctions in adult rat cardiomyocytes in culture. *Circ Res* 85(2): 154–167.
55. Luo Y, Radice GL (2003) Cadherin-mediated adhesion is essential for myofibril continuity across the plasma membrane but not for assembly of the contractile apparatus. *J Cell Sci* 116(Pt 8):1471–1479.
56. Matsuda T, et al. (2006) N-cadherin signals through Rac1 determine the localization of connexin 43 in cardiac myocytes. *J Mol Cell Cardiol* 40(4):495–502.
57. Li J, et al. (2016) LRP6 acts as a scaffold protein in cardiac gap junction assembly. *Nat Commun* 7:11775.
58. King JH, Huang CL, Fraser JA (2013) Determinants of myocardial conduction velocity: implications for arrhythmogenesis. *Front Physiol* 4:154.
59. Shah RV, et al. (2016) Diet and adipose tissue distributions: The Multi-Ethnic Study of Atherosclerosis. *Nutr Metab Cardiovasc Dis* 26(3):185–193.
60. Cui S, Ho WK, Kim ST, Cho H (2010) Agonist-induced localization of Gq-coupled receptors and G protein-gated inwardly rectifying K+ (GIRK) channels to caveolae determines receptor specificity of phosphatidylinositol 4,5-bisphosphate signaling. *J Biol Chem* 285(53):41732–41739.
61. Valiunas V, Beyer EC, Brink PR (2002) Cardiac gap junction channels show quantitative differences in selectivity. *Circ Res* 91(2):104–111.
62. Sung DJ, et al. (2012) Blockade of K+ and Ca2+ channels by azole antifungal agents in neonatal rat ventricular myocytes. *Biol Pharm Bull* 35(9):1469–1475.
63. Leem YE, Ha HL, Bae JH, Baek KH, Kang JS (2014) CDO, an Hh-coreceptor, mediates lung cancer cell proliferation and tumorigenicity through Hedgehog signaling. *PLoS One* 9(11):e111701.
64. Lee HJ, et al. (2015) Overweight in mice and enhanced adipogenesis in vitro are associated with lack of the hedgehog coreceptor boc. *Diabetes* 64(6):2092–2103.
65. Langmead B, Salzberg SL (2012) Fast gapped-read alignment with Bowtie 2. *Nat Methods* 9(4):357–359.
66. Gentleman RC, et al. (2004) Bioconductor: Open software development for computational biology and bioinformatics. *Genome Biol* 5(10):R80.
67. Knollmann BC, et al. (2006) Casq2 deletion causes sarcoplasmic reticulum volume increase, premature Ca2+ release, and catecholaminergic polymorphic ventricular tachycardia. *J Clin Invest* 116(9):2510–2520.